magnetochemistry

MDPI

Article

Slow Magnetic Relaxation and Luminescence Properties in Tetra β-Diketonate Lanthanide(III) Complexes

Saskia Speed [1], Ànnia Tubau [1], Ramon Vicente [1,*], Eva Castro [1] and Mercè Font-Bardia [2]

[1] Departament de Química Inorgànica i Orgànica, Universitat de Barcelona, Martí i Franquès 1-11, E-08028 Barcelona, Spain; saskiaspeedcastro@ub.edu (S.S.); anniatubau@ub.edu (À.T.); evacastroiniguez3@yahoo.es (E.C.)

[2] Departament de Mineralogia, Cristal·lografia i Dipòsits Minerals and Unitat de Difracció de R-X, Centre Científic i Tecnològic de la Universitat de Barcelona (CCiTUB), Universitat de Barcelona, Solé i Sabarís 1-3, E-08028 Barcelona, Spain; mercef@ccit.ub.edu

* Correspondence: rvicente@ub.edu; Tel.: +34-934039134; Fax: +34-93407725

Abstract: The reaction of $[Ln(btfa)_3(H_2O)_2]$ ($btfa^-$ = 4,4,4-trifluoro-1-phenyl-1,3-butanedionate) with additional 4,4,4-trifluoro-1-phenyl-1,3-butanedione (Hbtfa) and acridine (Acr) in ethanol allows the isolation of the mononuclear compounds $HAcr[Nd(btfa)_4]\cdot EtOH$, (**1**) and $HAcr[Ln(btfa)_4]$, Ln = Dy (**2**) and Yb (**3**); $HAcr^+$ = acridinium cation. Magnetic measurements indicate that complexes **1**–**3** show field-induced single-ion magnet behavior with anisotropy energy barriers and preexponential factors of U_{eff} = 20.7 cm^{-1}, $\tau_0 = 24.5 \times 10^{-8}$ s; U_{eff} = 40.5 cm^{-1}, $\tau_0 = 8.6 \times 10^{-10}$ s and U_{eff} = 22.7 cm^{-1}, $\tau_0 = 8.4 \times 10^{-8}$ s, for **1**–**3** respectively. The solid-state luminescence emission in the NIR region shows efficient energy transfer from the 4,4,4-trifluoro-1-phenyl-1,3-butanedionate ligands to the central Ln^{3+} ion in the case of compounds **1** and **3**.

Keywords: dysprosium(III); ytterbium(III); neodymium(III); beta-diketonate anion; magnetic properties; SMMs; luminescence; crystal structure

Citation: Speed, S.; Tubau, À.; Vicente, R.; Castro, E.; Font-Bardia, M. Slow Magnetic Relaxation and Luminescence Properties in Tetra β-Diketonate Lanthanide(III) Complexes. *Magnetochemistry* **2023**, *9*, 131. https://doi.org/10.3390/magnetochemistry9050131

Academic Editors: Matilde Fondo and Julio Corredoira-Vázquez

Received: 19 April 2023
Revised: 8 May 2023
Accepted: 12 May 2023
Published: 16 May 2023

1. Introduction

Lanthanide(III) compounds show interesting magnetic and luminescent properties derived from their partially filled *4f* valence shell. In the case of the magnetic properties, since the discovery of the first mononuclear lanthanide complexes of formula $[Pc_2Ln]^-\cdot TBA^+$ (Ln = Tb, Dy; Pc^{2-} = phthalocyanine dianion; TBA^+ = tetrabutylammonium) showing slow relaxation of the magnetization and acting as single-molecule magnets (SMMs) [1], a plethora of mono- and polynuclear SMM complexes derived from lanthanide ions with large orbital momentum and strong magnetic anisotropy have been reported [2–6]. In the field of molecular magnetism, the SMM compound $[Dy(Cp^{ttt})_2][B(C_6F_5)_4]$ (Cp^{ttt} = 1,2,4-tri-*tert*-butylcyclopentadienyl), exhibits a magnetic blocking temperature, T_B, of up to 60 K and an anisotropy barrier, U_{eff}, of 1837 cm^{-1} [7,8]. Another remarkable compound is the dysprosium metallocene cation $[(Cp^{iPr5})Dy(Cp^*)]^+$ (Cp^{iPr5} = penta-*iso*-propylcyclopentadienyl; Cp* = pentamethylcyclopentadienyl): T_B = 80 K and U_{eff} = 1541 cm^{-1}, pushing the blocking temperature higher than that of liquid nitrogen [9].

In addition to the above-mentioned magnetic properties, the lanthanide(III) ions also show intrinsic photoluminescent properties due to *4f*-*4f* electronic transitions, which result in long-lived emissions and narrow bandwidths. The lanthanide(III) ions have an incompletely filled *4f* subshell, which is shielded by the coordinated atoms due to the filled $5s^2$ and $5p^6$ orbitals, and hence, the emission transitions yield sharp lines characteristics of each element. However, the electronic *4f*–*4f* transitions are Laporte forbidden due to the parity selection rule, leading to low molar extinction coefficients ($\varepsilon < 10\ M^{-1}cm^{-1}$) for the direct photoexcitation of Ln(III) ions. To address this problem, it is necessary to use

organic chromophores that absorb energy and subsequently transfer it to the Ln(III) ion. This sensitization mechanism is commonly known as the "antenna effect" [10–12].

Thus, because of the characteristic narrow emission bands and long emission lifetimes of lanthanide(III) coordination compounds over a wide wavelength range (vis/near-IR) [13–24], these compounds show useful potential applications in telecommunications and biological imaging [25–30], and special attention has been directed towards Ln(III) compounds of Nd^{3+}, Er^{3+}, and Yb^{3+} as they exhibit near-infrared (NIR) emission [11–16,19–24].

In this regard, β-diketonates are among the most important "antenna ligands" owing to the following merits: (1) They show intense absorption from their conjugated π–π* transitions within a large wavelength range, (2) they have suitable triplet state energy levels (T1) to sensitize the emission of Ln(III) ions, (3) they can form stable adducts with Ln(III) ions through O,O bidentate chelating modes [31–36].

The interest in multifunctional materials showing SMM and luminescence properties is increasing [13,14,37]. We have previously published a series of multifunctional Nd(III) coordination complexes [38] derived from the β-diketonate ligand 4,4,4-trifluoro-1-(2-naphthyl)butane-1,3-dionato (ntfa) of formula $[Ln(ntfa)_3(ANCL)]$, (ANCL = ancillary ligand). We present now a new series of multifunctional materials showing SMM and luminescence properties derived from the 4,4,4-trifluoro-1-phenyl-1,3-butanedionate anion ($btfa^-$) with formula $HAcr[Ln(btfa)_4]$, where $HAcr^+$ = acridinium cation and Ln = Nd(III), Dy(III), and Yb(III) with the aim of studying the photophysical and magnetic behavior of the resulting compounds. By using as ligands four β-diketonate anions, the resulting $[Ln(btfa)_4]^-$ coordination compound has a high coordination number that excludes solvent molecules from the coordination sphere of the lanthanide(III) ions minimizing the deactivation by non-radiative processes. As far as we know, the acridinium cation has never been used as a countercation in the reported compounds of formula Cation[Ln(β-diketonate)$_4$] [39–46].

2. Experimental

2.1. Materials and Physical Measurements

4,4,4-trifluoro-1-phenyl-1,3-butanedione and acridine were purchased from Sigma-Aldrich. Lanthanide chloride hexahydrates and lanthanide(III) nitrate hexahydrates were obtained from Strem Chemicals. Infrared spectra (4000–400 cm^{-1}) were recorded from KBr pellets on a Perkin-Elmer 380-B spectrophotometer. The elemental analyses of the compounds were performed at the Serveis Científics i Tecnològics of the Universitat de Barcelona.

Powder X-ray diffraction, PXRD, measurements were used to check bulk phase purity. X-ray powder diffraction data were recorded at the Serveis Científics i Tecnològics of the Universitat de Barcelona with *PANalytical X'Pert PRO MPD θ/θ* powder diffractometer of 240 millimeters of radius in a configuration of a convergent beam with a focalizing mirror and a transmission geometry with flat samples sandwiched between low absorbing films Cu Kα radiation (λ = 1.5418 Å). Work power: 45 kV–40 mA. Incident beam slits defining a beam height of 0.4 mm. Incident and diffracted beam 0.02 radians *Soller* slits *PIXcel* detector: Active length = 3.347°. 2θ/θ scans from 2 to 70°2θ with a step size of 0.026°2θ and a measuring time of 298 s per step.

2.2. X-ray Crystal Structure Analysis

Crystallographic data for the structures were collected at 100(2) K on a Bruker D8 Venture diffractometer by use of Mo-Kα radiation. Crystallographic data of the three title complexes are summarized in Table 1. Following data reduction, Lp, and absorption corrections (programs APEX and SADABS) [47,48] and solution by direct methods, the structures were refined against F^2 with full-matrix least-squares using the program SHELX-2014 [49]. Anisotropic displacement parameters were employed for the non-hydrogen atoms. Hydrogen atoms were added at calculated positions and refined by use of a riding model with isotropic displacement parameters based on those of the parent atom.

Additional software: Mercury [50] and PLATON [51]. The full crystallographic data for the structures of complexes **1–3** have been deposited at the Cambridge Structural Database(CSD).

Table 1. Crystallographic data and processing parameters for **1–3**.

	1	**2**	**3**
Empirical formula	$C_{55}H_{39}F_{12}NdNO_9$	$C_{53}H_{34}DyF_{12}NO_8$	$C_{53}H_{34}YbF_{12}NO_8$
Formula Weight	1230.11	1203.31	1213.85
Crystal System	Triclinic	triclinic	triclinic
Space group	P-1 (No. 2)	P-1 (No. 2)	P-1 (No. 2)
a (Å)	10.1909 (3)	11.3753 (11)	11.3331 (5)
b (Å)	11.8183 (4)	13.2649 (14)	13.2428 (6)
c (Å)	11.9800 (4)	17.7231 (18)	17.7774 (9)
α (°)	110.310 (1)	91.029 (5)	90.509 (3)
β (°)	98.786 (1)	93.792 (5)	94.668 (3)
γ (°)	107.258 (1)	113.259 (5)	112.730 (2)
V ($Å^3$)	1238.44 (7)	2448.7 (4)	2450.3 (2)
Z	2	2	2
T (K)	100	100	100
μ (mm^{-1})	1.154	1.628	2.010
θ max (°)	30.7	27.5	26.4
Data collected	68,486	47,710	43,442
Unique refl./Rint	7617/0.043	11,242/0.171	10,031/0.154
Parameters/Restraints	357/3	649/2	676/0
S	1.11	1.03	1.03
R1/wR2 (all data)	0.0204/0.0525	0.0637/0.1293	0.0518/0.0912

2.3. Magnetic Measurements

Magnetic measurements were performed on solid polycrystalline samples in a Quantum Design MPMS-XL SQUID magnetometer at the Magnetic Measurements Unit of the Universitat de Barcelona. Pascal's constants were used to estimate the diamagnetic corrections, which were subtracted from the experimental susceptibilities to give the corrected molar magnetic susceptibilities.

2.4. Luminescence Measurements

Solid-state fluorescence spectra were recorded on a Horiva Jobin Yvon SPEX Nanolog fluorescence spectrophotometer equipped with a three-slit double-grating excitation and emission monochromator with dispersions of 2.1 nm/mm (1200 grooves/mm) at room temperature. The steady-state luminescence was excited by unpolarized light from a 450 W xenon CW lamp and detected at an angle of 90° for solid-state measurement by a red-sensitive Hamamatsu R928 photomultiplier tube. Spectra were reference corrected for both the excitation source light intensity variation (lamp and grating) and the emission spectral response (detector and grating). Near infra-red spectra were recorded at an angle of 90° using a liquid nitrogen-cooled, solid indium/gallium/arsenic detector (850–1600 nm).

2.5. Syntheses of the Complexes

2.5.1. $[Ln(btfa)_3(H_2O)_2]$

To synthesize the precursor compounds of formula $[Ln(btfa)_3(H_2O)_2]$ we have used the next procedure:

Thirty milliliters of a methanolic solution of $LnCl_3 \cdot 6H_2O$ (1 mmol) were added to 40 mL of another methanolic solution of 4,4,4-trifluoro-1-phenyl-1,3-butanedione (Hbtfa) (648 mg, 3 mmol) and sodium hydroxide (NaOH) (120 mg, 3 mmol). After 1 h stirring, 130 mL of deionized water were added, and the mixture was stirred overnight and then filtered and dried under vacuum.

2.5.2. $HAcr[Nd(btfa)_4] \cdot EtOH$ (1)

Ten milliliters of an ethanolic solution of $[Nd(btfa)_3(H_2O)_2]$ (206 mg, 0.25 mmol) were added to 10 mL of an ethanolic solution of Hbtfa (54 mg, 0.25 mmol) and acridine (Acr) (45 mg, 0.25 mmol). The mixture was stirred for 30 min, and then it was filtered, obtaining a yellow-green solution. The solution was left to stand undisturbed to form single crystals suitable for X-ray diffraction after 12 days. Yield: 76%. Anal.Calc. (%) for $C_{55}H_{40}F_{12}NdNO_9$ **1** C, 53.70; H, 3.25; N, 1.14. Exp.: C, 52.8; H, 2.8; N, 1.2. Infra-Red spectra (cm^{-1}): 1610 (s), 1580 (s), 1530 (m), 1490 (m), 1460 (m), 1320 (m), 1290 (s), 1240 (m), 1180 (s), 1130 (s), 1070 (m), 1020 (w), 941 (w), 752 (split, m), 701 (s), 630 (s), 599 (m), 579 (s).

2.5.3. $HAcr[Dy(btfa)_4]$ (2)

An ethanolic solution (10 mL) containing $[Dy(btfa)_3(H_2O)_2]$ (114 mg, 0.25 mmol) was added to another ethanolic solution (10 mL) of 4,4,4-trifluoro-1-phenyl-1,3-butanedione (Hbtfa) (54 mg, 0.25 mmol) and acridine (45 mg, 0.25 mmol). The mixture was stirred for 30 min, and then it was filtered. The mixture was left to stand undisturbed to form yellow single crystals suitable for X-ray analysis after two weeks. Yield: 45%. Anal.Calc. (%) for $C_{53}H_{34}DyF_{12}NO_8$ **2** C, 52.90; H, 2.85; N, 1.16. Found: C, 51.3; H, 2.8; N, 1.3. Infra-Red spectra (cm^{-1}): 1610 (s), 1570 (s), 1540 (m), 1490 (m), 1460 (m), 1320 (m), 1290 (s), 1240 (m), 1180 (s), 1130 (s), 1080 (m), 1020 (w), 943 (w), 750 (split, m), 701 (s), 631 (s), 580 (m), 519 (s).

2.5.4. $HAcr[Yb(btfa)_4]$ (3)

An ethanolic solution (10 mL) containing $[Yb(btfa)_3(H_2O)_2]$ (mg, 0.25 mmol) was added to another ethanolic solution (10 mL) of 4,4,4-trifluoro-1-phenyl-1,3-butanedione (Hbtfa) (54 mg, 0.25 mmol) and acridine (45 mg, 0.25 mmol). The mixture was stirred for 30 min and then it was filtered. The mixture was left to stand undisturbed to form single yellow crystals suitable for X-ray diffraction after two weeks. Yield: 36%. Anal.Calc. (%) for $C_{53}H_{34}YbF_{12}NO_8$ **3** C, 52.44; H, 2.82; N, 1.15. Found: C, 52.6; H, 3.0; N, 1.2. Infra-Red spectra (cm^{-1}): 1610 (s), 1580 (s), 1530 (m), 1490 (m), 1470 (m), 1320 (m), 1290 (s), 1240 (m), 1180 (s), 1130 (s), 1080 (m), 1020 (w), 941 (w), 750 (split, m), 699 (s), 632 (s), 580 (m), 572 (s).

The isolated complexes **1**–**3** were structurally characterized by single-crystal X-ray crystallography as well as by elemental microanalyses and by IR spectroscopy. Moreover, their purity was checked by Powder X-ray Diffraction (PXRD, Figure S1 in the Supplementary Section).

As expected, the IR spectra of complexes **1**–**3** display a general characteristic feature. The strong vibrational band observed over the frequency range 1605–1615 cm^{-1} is typically assigned to the coordinated carbonyl stretching frequency, ν(C=O).

3. Results and Discussion

3.1. Description of the Crystal Structures

Complex $HAcr[Nd(btfa)_4] \cdot EtOH$, **1** crystallizes in the triclinic space group P-1 (n°2). A partially labeled plot of the structure of compound **1** is shown in Figure 1. Selected bond distances and angles are listed in Table 2. The structure consists of $[Nd(btfa)_4]^-$ anions, $HAcr^+$ cations, and an ethanol molecule. In the anion of **1**, the central Nd(III) ion is coordinated to four bidentate 4,4,4-trifluoro-1-phenyl-1,3-butanedionate ($btfa^-$) ligands.

The Nd-O distances are in the range 2.434–2.460 Å. The acridinium cation and ethanol molecule are connected to the complex ion through a hydrogen bond each (N1—H22···O3 and O5—H5···O1, respectively). The structure of **1** presents symmetry disorder both in the ethanol molecule and in the acridinium cation.

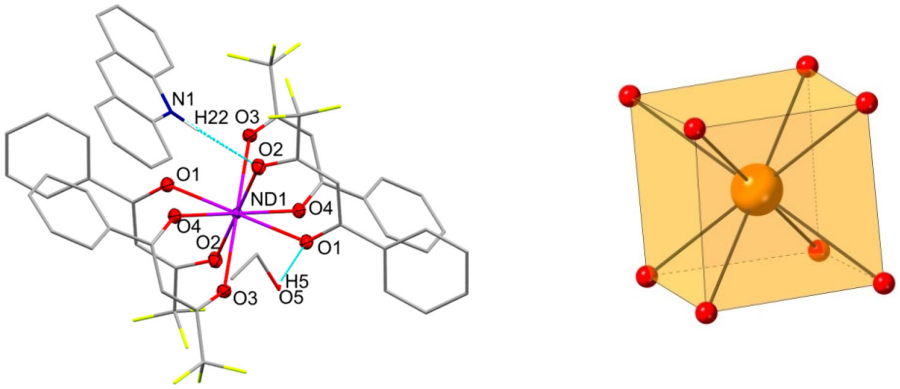

Figure 1. Perspective view (**left**) and coordination figure (**right**) of **1.** Hydrogen atoms have been omitted for clarity. Color code, pink: Neodymium, red: Oxygen, dark blue: Nitrogen, grey: Carbon, green: Fluorine.

Table 2. Selected bond distances (Å) and angles (°) for 1–3.

	1		**2**	**3**
Nd1-O1	2.4335 (11)	Ln1-O1	2.379 (4)	2.278 (4)
Nd1-O2	2.4600 (11)	Ln1-O2	2.330 (4)	2.302 (4)
Nd1-O3	2.4501 (11)	Ln1-O3	2.394 (4)	2.297 (4)
Nd1-O4	2.4405 (11)	Ln1-O4	2.326 (4)	2.291 (4)
Nd1-O1_$1	2.4335 (11)	Ln1-O5	2.348 (4)	2.366 (4)
Nd1-O2_$1	2.4600 (11)	Ln1-O6	2.322 (4)	2.279 (4)
Nd1-O3_$1	2.4501 (11)	Ln1-O7	2.316 (4)	2.341 (4)
Nd1-O4_$1	2.4405 (11)	Ln1-O8	2.332 (4)	2.283 (4)
O1-Nd1-O2	69.46 (4)	O1-Ln1-O2	71.69 (15)	75.08 (14)
O1-Nd1-O3	71.05 (3)	O1-Ln1-O3	77.34 (13)	140.44 (13)
O1-Nd1-O4	110.28 (4)	O1-Ln1-O4	77.53 (13)	76.22 (13)
O1-Nd1-O1_$1	180.00	O1-Ln1-O5	148.85 (13)	148.13 (13)
O1-Nd1-O2_$1	110.54 (4)	O1-Ln1-O6	129.30 (16)	104.65 (15)
O1-Nd1-O3_$1	108.96 (3)	O1-Ln1-O7	72.57 (13)	72.47 (13)
O1-Nd1-O4_$1	69.72 (4)	O1-Ln1-O8	128.83 (14)	86.02 (14)
O2-Nd1-O3	108.05 (4)	O2-Ln1-O3	78.75 (14)	72.86 (13)
O2-Nd1-O4	71.88 (3)	O2-Ln1-O4	142.25 (13)	75.82 (13)
O1_$1-Nd1-O2	110.54 (4)	O2-Ln1-O5	103.14 (15)	122.90 (13)
O2-Nd1-O2_$1	180.00	O2-Ln1-O6	144.99 (13)	147.44 (13)
O2-Nd1-O3_$1	71.95 (4)	O2-Ln1-O7	86.18 (15)	131.50 (13)
O2-Nd1-O4_$1	108.12 (3)	O2-Ln1-O8	69.31 (14)	69.70 (13)
O3-Nd1-O4	69.12 (4)	O3-Ln1-O4	73.57 (15)	73.96 (14)
O1_$1-Nd1-O3	108.96 (3)	O3-Ln1-O5	71.55 (13)	70.85 (13)
O2_$1-Nd1-O3	71.95 (4)	O3-Ln1-O6	128.82 (13)	90.64 (14)

Table 2. *Cont.*

	1		2	3
O3-Nd1-O3_$1	180.00	O3-Ln1-O7	149.32 (12)	147.10 (13)
O3-Nd1-O4_$1	110.88 (4)	O3-Ln1-O8	124.29 (16)	103.72 (15)
O1_$1-Nd1-O4	69.72 (4)	O4-Ln1-O5	91.99 (14)	130.85 (13)
O2_$1-Nd1-O4	108.12 (3)	O4-Ln1-O6	72.48 (14)	72.65 (13)
O3_$1-Nd1-O4	110.88 (4)	O4-Ln1-O7	105.08 (15)	127.94 (15)
O4-Nd1-O4_$1	180.00	O4-Ln1-O8	148.35 (14)	144.28 (13)
O1_$1-Nd1-O2_$1	69.46 (4)	O5-Ln1-O6	72.57 (15)	74.56 (13)
O1_$1-Nd1-O3_$1	71.05 (3)	O5-Ln1-O7	138.52 (13)	76.54 (13)
O1_$1-Nd1-O4_$1	110.28 (4)	O5-Ln1-O8	72.92 (15)	77.95 (13)
O2_$1-Nd1-O4_$1	108.05 (4)	O6-Ln1-O7	77.00 (14)	76.39 (14)
O2_$1-Nd1-O4_$1	71.88 (3)	O6-Ln1-O8	76.44 (15)	142.66 (13)
O3_$1-Nd1-O4_$1	69.12 (4)	O7-Ln1-O8	73.04 (16)	72.98 (14)

Symmetry code $1: 1−x, 1−y, 1−z.

Complex HAcr[Dy(btfa)$_4$] **2** crystallizes in the triclinic space group P-1 (n°2). A partially labeled plot of the structure of compound **2** is shown in Figure 2. Selected bond distances and angles are listed in Table 2. The structure consists of [Dy(btfa)$_4$]$^-$ anions and HAcr$^+$ cations. In the anion of **2**, the central Dy(III) ion is coordinated to four bidentate 4,4,4-trifluoro-1-phenyl-1,3-butanedionate (btfa$^-$) ligands. The Dy-O distances are in the range 2.316–2.394 Å. The acridinium cation is connected to the complex ion through a hydrogen bond (N1—H1A . . . O3).

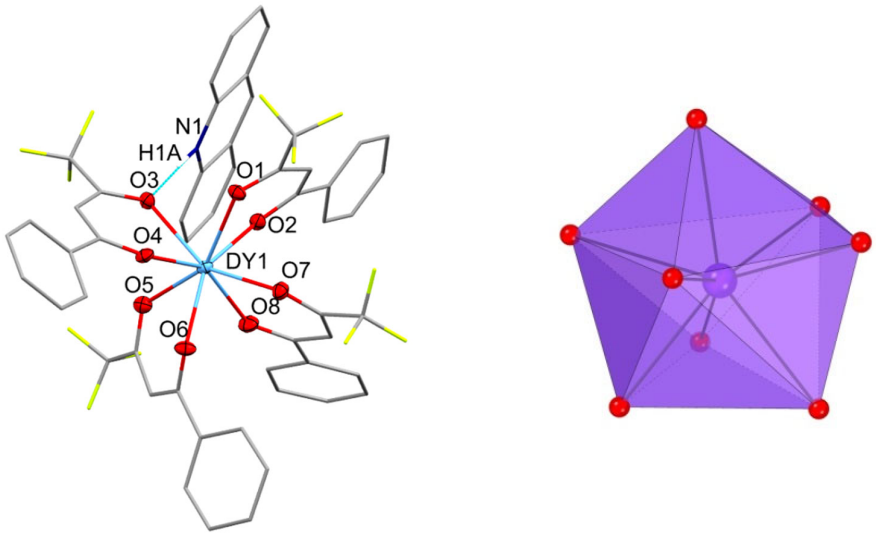

Figure 2. Perspective view (**left**) and coordination figure (**right**) of **2**. The hydrogen atoms are omitted for better clarification. Color code, light blue: Dysprosium, red: Oxygen, dark blue: Nitrogen, grey: Carbon, green: Fluorine.

Complex HAcr[Yb(btfa)$_4$] **3** crystallizes in the triclinic space group P-1 (n°2). A partially labelled plot of the structure of compound **3** is shown in Figure 3. Selected bond distances and angles are listed in Table 2. The structure consists of [Yb(btfa)$_4$]$^-$ anions and HAcr$^+$ cations. In the anion of **3**, the central Yb(III) ion is coordinated to four bidentate 4,4,4-trifluoro-1-phenyl-1,3-butanedionate (btfa$^-$) ligands. The Yb-O distances are in the range 2.278–2.366 Å. The acridinium cation is connected to the complex ion through a hydrogen bond (N1—H1···O5).

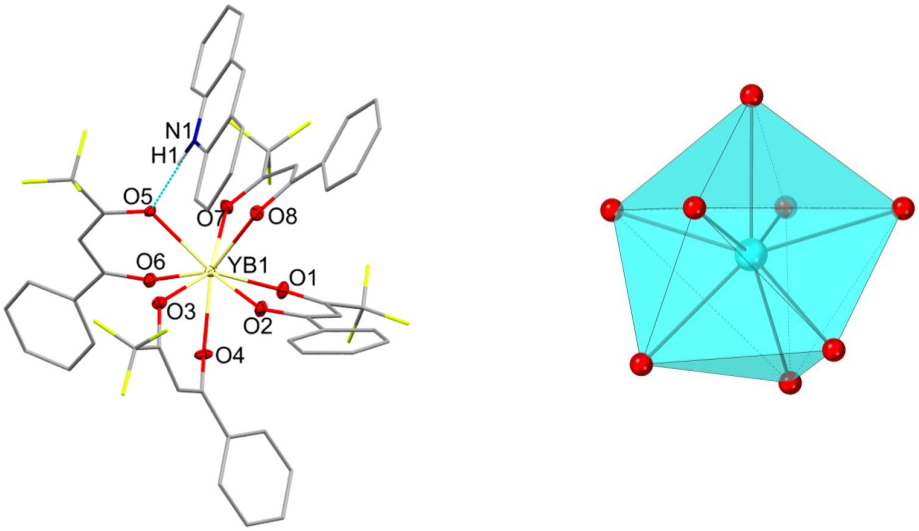

Figure 3. Perspective view (**left**) and coordination figure (**right**) of **3.** Hydrogen atoms have been omitted for clarity. Color code, yellow: Ytterbium, red: Oxygen, dark blue: Nitrogen, grey: Carbon, green: Fluorine.

This family of $[Ln(btfa)_4]^-$ complexes provides an opportunity to study the influence of lanthanide contraction over the structural arrangement [52]. When the atomic number of the metal increases, the radius of the Ln(III) cations decreases, and the Ln-O bond lengths decrease due to the increase of the lanthanide contraction along the period (Table 2).

The SHAPE software [53,54] was used to determine the degree of distortion of the LnO_8 coordination polyhedra in complexes **1**–**3**. The lowest continuous shape measurements (CShM's) value for **1** (0.026) corresponds to a cubic geometry, CU-8 (O_h). However, the lowest continuous shape measurements (CShM's) values for **2** and **3** correspond to a triangular dodecahedron, TDD-8 (D_{2d}), with values of 0.360 and 0.422 for **2** and **3,** respectively. CShM's values for **1**–**3** are listed in Table S1 (Supplementary Section). The metal coordination geometry for **1**–**3** is shown in Figures 1–3 (right), respectively. The three complexes under investigation reveal the existence of two types of metal coordination geometries for LnO_8: cube, CU-8 (O_h) for the Nd(III) compound **1** and triangular dodecahedron, TDD-8 (D_{2d}) for the Dy(III) and Yb(III) compounds **2** and **3,** respectively. The cube geometry for NdO_8 compared with the triangular dodecahedron for DyO_8 and YbO_8 is probably due to the slightly larger radius of the Nd(III) ion. As structural precedents, in the previously published compound of formula $(Hex_4N)[Nd(DBM)_4]$, Hex_4N = tetrahexylammonium, HDBM = dibenzoylmethane, the metal coordination geometry for NdO_8 is SAPR-8, (D_{4d}), square antiprism with a CShM value of 0.488. The Dy(III) analogous $(Hex_4N)[Nd(DBM)_4]$ also has a metal coordination geometry closest to a square antiprism with a CShM value of 0.287 [39]. In the Cation[Ln(β-diketonate)$_4$] compounds, the metal coordination geometries for LnO_8 are difficult to be predicted: By changing the β-diketonate ligand and the cation, we have clear structural changes in the central atom coordination geometry.

3.2. Magnetic Properties

3.2.1. DC Magnetic Susceptibility Studies

Direct current (dc) magnetic susceptibility (χ_M) data on polycrystalline powder samples of complexes **1**–**3** were collected under applied fields of 0.3 T over the temperature range 300–2 K.

The data for compounds **1**–**3** are plotted as $\chi_M T$ *vs.* T in Figure 4 (left). The room temperature $\chi_M T$ values are 1.57, 14.23, and 6.62 $cm^3 \cdot K \cdot mol^{-1}$, which are in agreement with the calculated values ($\chi_M T = N\mu_B{}^2 g_J{}^2 J(J+1)/3k_B$ where N: Avogadro constant; k_B: Bohr magneton; k_B: Boltzmann constant) of 1.64, 14.17, and 7.15 $cm^3 \cdot K \cdot mol^{-1}$ for one isolated Ln(III) ion [55].

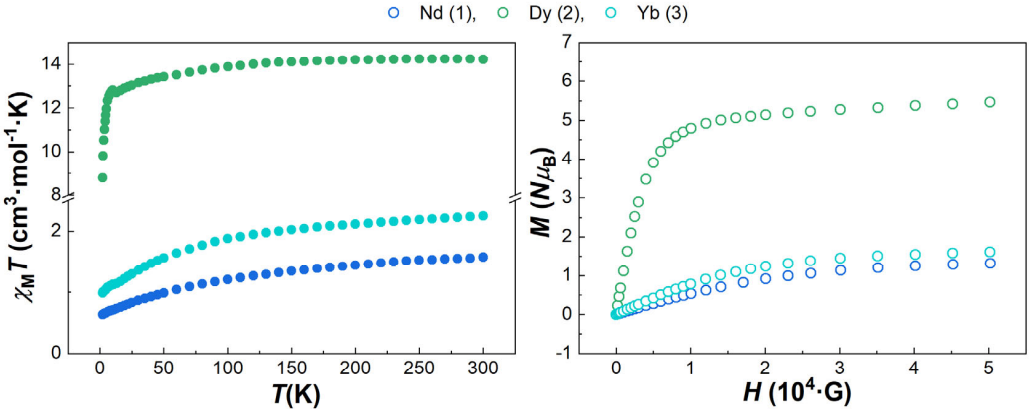

Figure 4. $\chi_M T$ vs. T plots for compounds **1–3** (**left**) and magnetization plots measured at T = 2 K (field dependence of **1–3**) (**right**).

Upon cooling, the $\chi_M T$ values of **1** and **3** gradually decrease, which should be mainly attributed to the thermal depopulation of the crystal field sublevels. At 2.0 K, the corresponding $\chi_M T$ values are 0.63 and 4.89 cm^3·K·mol^{-1}.

On the other hand, for **2** the $\chi_M T$ values upon cooling remain almost constant down to ca. 8 K and then decrease rapidly down to 8.79 cm^3·K·mol^{-1} at 2.0 K.

Isothermal field-dependent magnetization measurements were performed on all complexes, **1–3**, at 2 K and are depicted in Figure 4 (right). The magnetization of compounds **1–3** rises fast under low fields and then slowly under high fields before reaching values of 5.46, 6.29, and 1.61μ_B, respectively. None of the presented compounds reach saturation of the magnetization values at the highest applied magnetic fields. The saturations of magnetization values for mononuclear Nd^{3+}, Dy^{3+}, and Yb^{3+} compounds would be ($g_J \times J$): 3.27, 10, and 30.45 μ_B, respectively.

3.2.2. Ac Magnetic Susceptibility Studies

To study if the complexes under investigation may show SMM behavior, dynamic magnetic studies were performed on compounds **1–3**. The measurements reveal that at zero static external magnetic field none of the complexes show out-of-phase (χ_M'') signals of the ac susceptibility at frequencies up to 1488 Hz. This fact may indicate a low magnetic anisotropy or that at zero dc field, the Quantum tunneling of magnetization, QTM, process dominates the magnetization relaxation time (τ), but this process can be suppressed or partially suppressed at low temperatures when a static magnetic field is applied [56].

For **1–3** frequency dependence of χ_M'' reveals temperature-dependent peaks when a dc field of 0.10 T is applied under a 4×10^{-4} T ac field oscillating at frequencies between 1 and 1488 Hz in the temperature range of 1.84–5.00 K for **1** (Figure 5a), 1.80–5.60 K for **2** (Figure 5d), and 1.88–5.00 K for **3** (Figure 5g).

AC susceptibility frequency dependences of both χ_M' and χ_M'' were analyzed for **1–3** using the generalized Debye model, Equation (S1) [57]. The representation of the corresponding Cole–Cole plots (Figure 5b,e,h) estimated α values close to zero (see Tables S2–S4 for compounds **1–3**, respectively), revealing a single relaxation process for these compounds [58]. Only the χ_M'' vs. frequency curves showing maximum values were analyzed using the Generalized Debye model.

The temperature dependence of the relaxation times (τ) (Figure 5c,f,i) shows that at temperatures above 2.2, 3.1, and 2.3 K for **1–3**, respectively, the rate of τ follows the Arrhenius law [$\tau^{-1} = {\tau_0}^{-1}\exp(-U_{eff}/k_BT)$], leading to effective energy barriers (U_{eff}) and pre-exponential factors (τ_0) of 20.7 cm^{-1} and $4.5 \cdot 10^{-8}$ s^{-1} (**1**), 40.5 cm^{-1} and $8.6 \cdot 10^{-10}$ s^{-1} (**2**), and 22.7 cm^{-1} and $8.4 \cdot 10^{-8}$ s^{-1} (**3**).

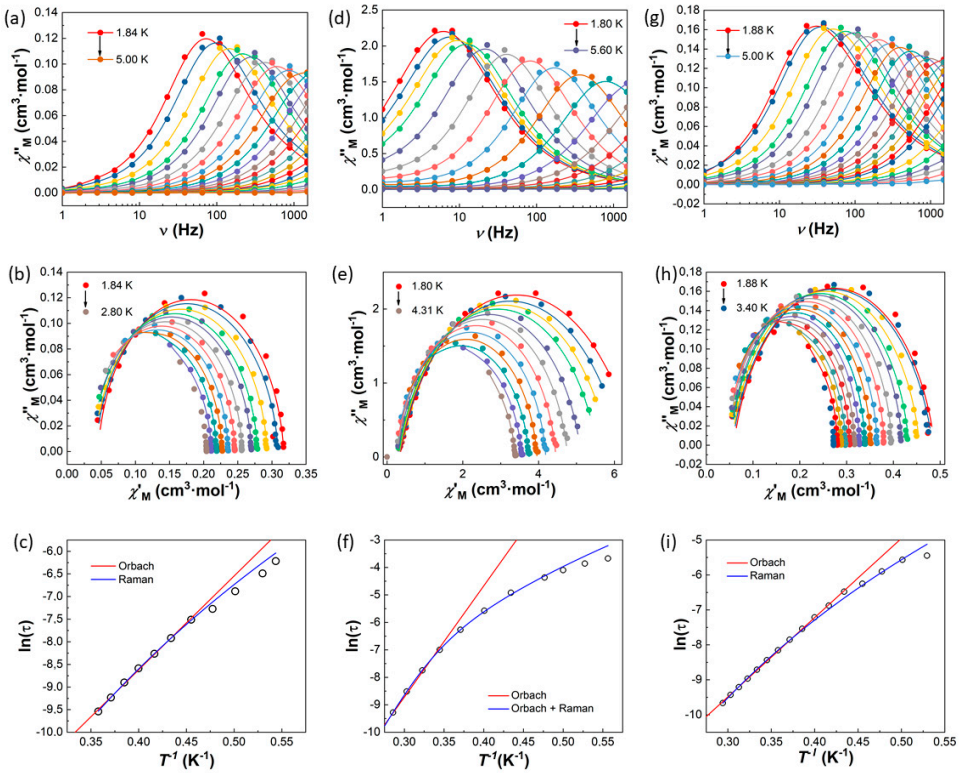

Figure 5. Top: Frequency dependence of the χ_M'' component for **1** (**a**), for **2** (**d**), and for **3** (**g**). The dots represent the experimental points obtained in the measurement, and the continuous line are guide for the eyes. **Middle**: Cole–Cole plot of compounds **1** (**b**), **2** (**e**), and **3** (**h**). The dots represent the χ_M' and χ_M'' values obtained in the measurements, and the solid lines represent the fitting using generalized Debye models. **Bottom**: Magnetization relaxation time [ln(τ)] vs. T^{-1} for **1** (**c**), for **2** (**f**), and for **3** (**i**). Solid lines represent the best theoretical fittings (see text).

Nevertheless, the thermal dependences of τ at low temperatures deviate from the linearity of the thermal Orbach process in the three compounds. Therefore, these data were first fitted accounting for Orbach, direct, and Raman relaxation processes by using the expression:

$$\tau^{-1} = {\tau_0}^{-1} \exp(-U_{eff}/k_BT) + AT + CT^n$$

However, we found that the relaxation rate at low temperatures of compounds **1** and **3** could be very well simulated by using the equation for a Raman-only relaxation process $\tau^{-1} = CT^n$ and compound **2** without the direct process using the equation $\tau^{-1} = \tau_0 \exp(-U_{eff}/k_BT) + CT^n$. The best fit parameters resulted in C = 2.6(3) $s^{-1}\cdot K^{-n}$ and n = 8.3(1) for **1**, C = 1.23(8) $s^{-1}\cdot K^{-n}$ and n = 7.73(5) for **3**, and $\tau_0 = 3.4\cdot10^{-11}$ s^{-1}, U_{eff} = 53.0(5) cm^{-1}, C = 0.38(9) $s^{-1}\cdot K^{-n}$, and n = 7.1(2) for **2**.

3.3. Luminescence Properties

3.3.1. HAcr[Nd(btfa)$_4$]·EtOH **1**

For compound **1** the excitation spectrum recorded at λ_{em} = 1021 nm shows the π→π* transition of the ligand. The emission spectrum recorded at λ_{ex} = 364 nm in the UV-visible range shows a broad band between 430 and 672 nm, which corresponds to the emission of the counterion $HAcr^+$ [59–61]. The emission spectrum (λ_{exc} = 364 nm) of compound **1** in the NIR range shows the emission bands at 883, 1052, and 1323 nm that correspond to the transitions $^4I_J \leftarrow {}^4F_{3/2}$ with J: 9/2, 11/2, and 13/2, respectively [55]. The excitation and emissions (both in the visible and the NIR range) spectra are depicted in Figure 6.

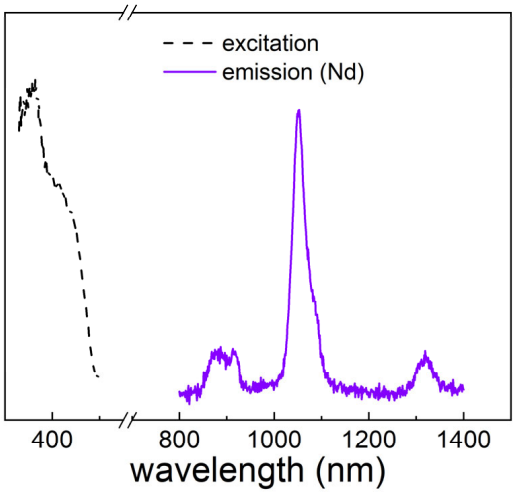

Figure 6. Excitation (dashed line) and emission (solid line) spectra of **1**.

3.3.2. HAcr[Dy(btfa)$_4$] **2**

The emission and excitation spectra of compound **2** were recorded at λ_{ex} = 361 nm and λ_{em} = 560 nm and are shown in Figure 7. For this compound, we can only observe the excitation and emission bands that correspond to the $HAcr^+$ cation, which are two broad bands between 300 and 469 nm and 435 and 676 nm, respectively. No bands are observed in the NIR range. Dysprosium ions show two characteristic emission bands in the visible range around 470 and 570 nm, corresponding to the $^4F_{9/2} \rightarrow {}^6H_J$ where J = 15/2 and 13/2 [55]. In the case of compound **2** these bands are masked by the absorption of the $HAcr^+$ molecule, which is a high-absorbing chromophore [59–61].

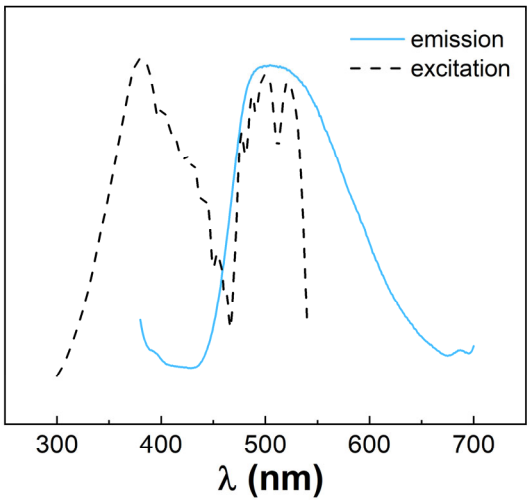

Figure 7. Excitation (dashed line) and emission (solid line) spectra of **2**.

3.3.3. HAcr[Yb(btfa)$_4$] **3**

For compound **3** the excitation spectrum recorded at λ_{em} = 1021 nm shows the $\pi \rightarrow \pi^*$ transition of the ligand. The emission spectrum recorded at λ_{ex} = 361 nm in the UV-visible range shows a broad band between 430 and 672 nm which corresponds to the emission of the counterion $HAcr^+$ [59–61]. In the NIR range, it shows an intense band centered at 1021 nm that corresponds to the $^2F_{5/2} \rightarrow {}^2F_{7/2}$ transition [55]. The excitation and emission spectra (both in the visible and the NIR range) are depicted in Figure 8.

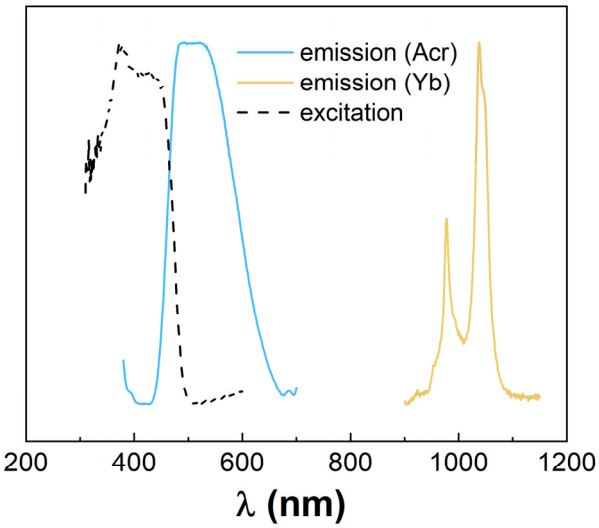

Figure 8. Excitation (dashed line) and emission (solid lines) spectra of **3**.

4. Conclusions

In this study, we report the synthesis and crystal structure of three eight-coordinated Ln(III) compounds of formula HAcr[Nd(btfa)$_4$]·EtOH, Nd (**1**) and HAcr[Ln(btfa)$_4$], Ln = Dy (**2**) and Yb (**3**); HAcr$^+$ = acridinium cation. btfa- = 4,4,4-trifluoro-1-phenyl-1,3-butanedionate (btfa). As far as we know, the acridinium cation has never been used as a countercation in the reported series of formula Cation[Ln(β-diketonate)$_4$]. Complexes **1**–**3** display the emission band that corresponds to the HAcr+ cation in the visible range, which is a broad band between 430 and 672 nm, and **1** and **3** the *f*-*f* emissions in the NIR region of the corresponding lanthanide ion. Additionally, the dynamic magnetic measurements performed below 10 K revealed field-induced SMM behavior for compounds **1**–**3**. Thus, compounds **1** and **3** can be considered to serve as bifunctional complexes, as they reveal both field-induced SMM and luminescent properties.

Supplementary Materials: The following supporting information can be downloaded at: https://www.mdpi.com/article/10.3390/magnetochemistry9050131/s1. Nd(**1**); CCDC 2249593, Dy(**2**) and CCDC 2249595, Yb(**3**) contain the crystallographic data in CIF format for **1**–**3**, respectively. More Supplementary Materials corresponding to PXRD patterns and Infra-red spectra of compounds **1**–**3** are presented as Supplementary Figures S1 and S2 respectively. Table S1 shows the Continuous shape measures (CShM's) values for **1**–**3**. Tables S2–S4 show the relaxation parameters values for the best fit of $\chi M''$ and $\chi M'$ in front of frequency using the one component generalized Debye model for compounds **1**–**3** respectively.

Author Contributions: Conceptualization, R.V. and S.S.; methodology, R.V., À.T. and S.S.; software, S.S., À.T., R.V. and M.F.-B.; validation, R.V.; investigation, E.C., À.T. and S.S.; resources, R.V.; data curation, S.S., À.T., R.V. and M.F.-B.; writing and editing manuscript, S.S., À.T. and R.V.; visualization, À.T., E.C., R.V. and S.S.; administration of project and supervision, R.V.; funding management, R.V. The authors agree with the manuscript version presented. All authors have read and agreed to the published version of the manuscript.

Funding: R.V., À.T. and S.S. are thankful to Ministerio de Ciencia, Innovación y Universidades (Spain), Project PGC2018-094031-B-100.

Institutional Review Board Statement: Not applicable.

Informed Consent Statement: Not applicable.

Data Availability Statement: Data is contained within the article or Supplementary Materials.

Acknowledgments: R.V., S.S. and À.T. acknowledge the financial support from the Ministerio de Ciencia, Innovación y Universidades (Spain) under Project PGC2018-094031-B-100.

Conflicts of Interest: The authors declare no conflict of interest.

References

1. Ishikawa, N.; Sugita, M.; Ishikawa, T.; Koshihara, S.Y.; Kaizu, Y. Lanthanide Double-Decker Complexes Functioning as Magnets at the Single-Molecular Level. *J. Am. Chem. Soc.* **2003**, *125*, 8694–8695. [CrossRef] [PubMed]
2. Tang, J.; Zhang, P. *Lanthanide Single Molecule Magnets*; Springer: Berlin/Heidelberg, Germany, 2015.
3. Feltham, H.L.C.; Brooker, S. Review of purely 4*f* and mixed-metal n*d*-4*f* single-molecule magnets containing only one lanthanide ion. *Coord. Chem. Rev.* **2014**, *276*, 1–33. [CrossRef]
4. Woodruff, D.N.; Winpenny, R.E.P.; Layfield, R.A. Lanthanide Single-Molecule Magnets. *Chem. Rev.* **2013**, *113*, 5110–5148. [CrossRef]
5. Zabala-Lekuona, A.; Seco, J.M.; Colacio, E. Single-Molecule Magnets: From Mn12-ac to dysprosium metallocenes, a travel in time. *Coord. Chem. Rev.* **2021**, *441*, 213984. [CrossRef]
6. Borah, A.; Murugavel, R. Magnetic relaxation in single-ion magnets formed by less-studied lanthanide ions Ce(III), Nd(III), Gd(III), Ho(III), Tm(II/III) and Yb(III). *Coord. Chem. Rev.* **2022**, *453*, 214288. [CrossRef]
7. Guo, F.-S.; Day, B.M.; Chen, Y.-C.; Tong, M.-L.; Mansikkamäki, A.; Layfield, R.A. A Dysprosium Metallocene Single-Molecule Magnet Functioning at the Axial Limit. *Angew. Chem. Int. Ed.* **2017**, *56*, 11445–11449. [CrossRef] [PubMed]
8. Goodwin, C.A.P.; Ortu, F.; Reta, D.; Chilton, N.F.; Mills, D.P. Molecular magnetic hysteresis at 60 kelvin in dysprosocenium. *Nature* **2017**, *548*, 439–442. [CrossRef]
9. Guo, F.-S.; Day, B.; Chen, Y.-C.; Tong, M.L.; Mansikkamäki, A.; Layfield, R.A. Magnetic hysteresis up to 80 kelvin in a dysprosium metallocene single-molecule magnet. *Science* **2018**, *362*, 1400–1403. [CrossRef]
10. Hasegawa, Y.; Kitagawa, Y.; Nakanish, T. Effective photosensitized, electrosensitized, and mechanosensitized luminescence of lanthanide complexes. *NPG Asia Mater.* **2018**, *10*, 52–70. [CrossRef]
11. Bünzli, J.-C.G. On the design of highly luminescent lanthanide complexes. *Coord. Chem. Rev.* **2015**, *293–294*, 19–47. [CrossRef]
12. De Sá, G.F.; Malta, O.L.; de Mello Donegá, C.; Simas, A.M.; Longo, R.L.; Santa-Cruz, P.A. Spectroscopic Properties and Design of Highly Luminescent Lanthanide Coordination Complexes. *Coord. Chem. Rev.* **2000**, *196*, 165–195. [CrossRef]
13. Huang, G.; Calvez, G.; Suffren, Y.; Daiguebonne, C.; Freslon, S.; Guillou, O.; Bernot, K. Closing the Circle of the Lanthanide-Murexide Series: Single-Molecule Magnet Behavior and Near-Infrared Emission of the Nd^{III} Derivative. *Magnetochemistry* **2018**, *4*, 44. [CrossRef]
14. Casanovas, B.; Font-Bardía, M.; Speed, S.; El Fallah, M.S.; Vicente, R. Field Induced SMM and Visible/NIR-luminescence behaviour for dinuclear Ln(III) complexes with 2-fluorobenzoate. *Eur. J. Inorg. Chem.* **2018**, *2018*, 1928–1937. [CrossRef]
15. Chen, H.-Y.; Wang, W.-M.; Gao, H.-L.; Cui, J.-Z. Near-infrared luminescence and SMM behaviors of a family of dinuclear lanthanide 8-quinolinolate complexes. *RSC Adv.* **2016**, *6*, 34165–34174.
16. Bala, S.; Bishwas, M.S.; Pramanik, B.; Khanra, S.; Fromm, K.M.; Poddar, P.; Mondal, R. Construction of Polynuclear Lanthanide (Ln = DyIII, TbIII, and NdIII) Cage Complexes Using Pyridine−Pyrazole-Based Ligands: Versatile Molecular Topologies and SMM Behavior. *Inorg. Chem.* **2015**, *54*, 8197–8206. [CrossRef]
17. Galán, L.A.; Wada, S.; Cameron, L.; Sobolev, A.N.; Hasegawa, Y.; Zysman-Colman, E.; Ogden, M.I.; Massi, M. Photophysical investigation of near infrared emitting lanthanoid complexes incorporating tris(2-naphthoyl)methane as a new antenna ligand. *Dalton Trans.* **2019**, *48*, 3768–3776. [CrossRef]
18. Yang, C.; Fu, L.M.; Wang, Y.; Zhang, J.P.; Wong, W.T.; Ai, X.-C.; Qiao, F.Y.; Zou, B.S.; Gui, L.-L. A Highly Luminescent Europium Complex Showing Visible-Light-Sensitized Red Emission: Direct Observation of the Singlet Pathway. *Angew. Chem. Int. Ed.* **2004**, *116*, 5120–5123. [CrossRef]
19. Imbert, D.; Cantuel, M.; Bunzli, J.-C.G.; Bernardinelli, G.; Piguet, C. Extending Lifetimes of Lanthanide-Based Near-Infrared Emitters (Nd, Yb) in the Millisecond Range through Cr(III) Sensitization in Discrete Bimetallic Edifices. *J. Am. Chem. Soc.* **2003**, *125*, 15698–15699. [CrossRef]
20. Beeby, A.; Burton-Pye, B.P.; Faulkner, S.; Motson, G.R.; Jeffery, J.C.; McCleverty, J.A.; Ward, M.D. Synthesis and near-IR luminescence properties of neodymium(III) and ytterbium(III) complexes with poly(pyrazolyl)borate ligands. *J. Chem. Soc. Dalton Trans.* **2002**, *9*, 1923–1928. [CrossRef]
21. Li, W.; Li, J.; Li, H.; Yan, P.; Hou, G.; Li, G. NIR luminescence of 2-(2,2,2-trifluoroethyl)-1-indone (TFI) neodymium and ytterbium complexes. *J. Lumin.* **2014**, *146*, 205–210. [CrossRef]
22. Wang, X.; Wang, L.; Luo, Y.; Wu, W.; Tian, X.; Zhang, Q.; Chen, B. NIR luminescence of a visible-light-sensitized neodymium complex with large experimental fluorescence branching ratio for $4F_{3/2} \rightarrow 4I_{11/2}$ in PMMA. *J. Mater. Res.* **2011**, *26*, 1517–1523. [CrossRef]
23. Bennett, S.D.; Pope, S.J.A.; Ward, B.D. Near-IR luminescent neodymium complexes: Spectroscopic probes for hydroamination catalysis. *Chem. Commun.* **2013**, *49*, 6072–6074. [CrossRef]
24. Shavaleev, N.M.; Scopelliti, R.; Gumy, F.; Bünzli, J.-C.G. Near-Infrared Luminescence of Nine-Coordinate Neodymium Complexes with Benzimidazole-Substituted 8-Hydroxyquinolines. *Inorg. Chem.* **2008**, *47*, 9055–9068. [CrossRef]
25. Comby, S.; Bünzli, J.-C.G. Lanthanide near-infrared luminescence in molecular probes and devices. In *Handbook on the Physics and Chemistry of Rare Earths*; Elsevier: Amsterdam, The Netherlands, 2007; Volume 37, pp. 217–470.

26. Hasegawa, Y.; Nakanishi, T. Luminescent lanthanide coordination polymers for photonic applications. *RSC Adv.* **2015**, *5*, 338–353. [CrossRef]
27. Hasegawa, Y. Photofunctional Lanthanoid Complexes, Coordination Polymers, and Nanocrystals for Future Photonic Applications. *Bull. Chem. Soc. Jpn.* **2014**, *87*, 1029–1057. [CrossRef]
28. Liu, J.-L.; Chen, Y.-C.; Tong, M.-L. Symmetry strategies for high performance lanthanide-based single-molecule magnets. *Chem. Soc. Rev.* **2018**, *47*, 2431–2453. [CrossRef] [PubMed]
29. Eliseeva, S.V.; Bünzli, J.-C.G. Lanthanide luminescence for functional materials and bio-sciences. *Chem. Soc. Rev.* **2010**, *39*, 189–227. [CrossRef]
30. Bünzli, J.-C.G. Luminescence bioimaging with lanthanide complexes. In *Luminescence of Lanthanide Ions in Coordination Compounds and Nanomaterials*; De Bettencourt-Dias, A., Ed.; John Wiley & Sons: Chichester, UK, 2014; Chapter 4; pp. 125–196.
31. Ding, Y.; Wang, Y.; Li, H.; Duan, Z.; Zhang, H.; Zheng, Y. Photostable and efficient red-emitters based on zeolite L crystals. *J. Mater. Chem.* **2011**, *21*, 14755–14759. [CrossRef]
32. Ilmi, R.; Kanslz, S.; Dege, N.; Khan, M.S. Synthesis, structure, Hirshfeld surface analysis and photophysical studies of red emitting europium acetylacetonate complex incorporating a phenanthroline derivative. *J. Photochem. Photobiol. A* **2019**, *377*, 268–281. [CrossRef]
33. Da Rosa, P.P.F.; Kitagawa, Y.; Hasegawa, Y. Luminescent lanthanide complex with seven-coordination geometry. *Coord. Chem. Rev.* **2020**, *406*, 213153. [CrossRef]
34. Ahmed, Z.; Iftikhar, K. Red, orange-red and near-infrared light emitting ternary lanthanide tris β-diketonate complexes with distorted C_{4v} geometrical structures. *Dalton Trans.* **2019**, *48*, 4973–4986. [CrossRef]
35. Li, J.; Li, H.; Yan, P.; Chen, P.; Hou, G.; Li, G. Synthesis, Crystal Structure, and Luminescent Properties of 2-(2,2,2-Trifluoroethyl)-1-indone Lanthanide Complexes. *Inorg. Chem.* **2012**, *51*, 5050–5057. [CrossRef]
36. Ilmi, R.; Khan, M.S.; Li, Z.; Zhou, L.; Wong, W.-Y.; Marken, F.; Raithby, P.R. Utilization of Ternary Europium Complex for Organic Electroluminescent Devices and as a Sensitizer to Improve Electroluminescence of Red-Emitting Iridium Complex. *Inorg. Chem.* **2019**, *58*, 8316–8331. [CrossRef]
37. Long, J.; Guari, Y.; Ferreira, R.A.S.; Carlos, L.D.; Larionova, J. Recent advances in luminescent lanthanide based Single-Molecule Magnets. *Coord. Chem. Rev.* **2018**, *363*, 57–70. [CrossRef]
38. Vicente, R.; Tubau, À.; Speed, S.; Mautner, F.A.; Bierbaumer, F.; Fischer, R.C.; Massoud, S.S. Slow magnetic relaxation and luminescence properties in neodymium(III) 4,4,4-trifluoro-1-(2-naphthyl)butane-1,3-dionato complexes incorporating bipyridyl ligands. *New J. Chem.* **2021**, *45*, 14713–14723. [CrossRef]
39. Wu, Z.; Tian, Y.-M.; Chen, P.; Sun, W.-B.; Wang, B.-W.; Gao, S. A series of counter cation-dependent tetra β-diketonate mononuclear lanthanide(III) single-molecule magnets and immobilization on pre-functionalised GaN substrates by anion exchange reaction. *J. Mater. Chem. C* **2021**, *9*, 6911–6922.
40. Visconti, M.; Maggini, S.; Ciani, G.; Mercandelli, P.; Del Secco, B.; Prodi, L.; Sgarzi, M.; Zaccheroni, N.; Carlucci, L. New Lanthanide Metalloligands and Their Use for the Assembly of Ln–Ag Bimetallic Coordination Frameworks: Stepwise Modular Synthesis, Structural Characterization, and Optical Properties. *Cryst. Growth Des.* **2019**, *19*, 5376–5389. [CrossRef]
41. Akerboom, S.; Meijer, M.S.; Siegler, M.A.; Fu, W.T.; Bouwman, E. Structure, photo- and triboluminescence of the lanthanoid dibenzoylmethanates: $HNEt_3[Ln(dbm)_4]$. *J. Lumin.* **2014**, *145*, 278–282. [CrossRef]
42. Pointillart, F.; Maury, O.; Le Gal, Y.; Golhen, S.; Cador, O.; Ouahab, L. 4-(2-Tetrathiafulvalenyl-ethenyl)pyridine (TTF−CH==CH−Py) Radical Cation Salts Containing Poly(β-diketonate) Rare Earth Complexes: Synthesis, Crystal Structure, Photoluminescent and Magnetic Properties. *Inorg. Chem.* **2009**, *48*, 7421–7429. [CrossRef]
43. Navarro, Y.; Guedes, G.P.; Cano, J.; Oon, P.; Iglesias, M.J.; Lloret, F.; Lopez-Ortiz, F. Synthesis, structural characterization and electrochemical and magnetic studies of $M(hfac)_2$ (M = Cu^{II}, Co^{II}) and $Nd(hfac)_3$ complexes of 4-amino-TEMPO. *Dalton Trans.* **2020**, *49*, 6280–6294. [CrossRef]
44. Speed, S.; Pointillart, F.; Mulatier, J.-C.; Guy, L.; Golhen, S.; Cador, O.; le Guennic, B.; Riobe, F.; Maury, O.; Ouahab, L. Photophysical and Magnetic Properties in Complexes Containing 3d/4f Elements and Chiral Phenanthroline-Based Helicate-Like Ligands. *Eur. J. Inorg. Chem.* **2017**, *2017*, 2100–2111. [CrossRef]
45. Cary, S.K.; Livshits, M.; Cross, J.N.; Ferrier, M.G.; Mocko, V.; Stein, B.W.; Korimor, S.A.; Scott, B.L.; Rack, J.J. Advancing Understanding of the +4 Metal Extractant Thenoyltrifluoroacetonate (TTA^-); Synthesis and Structure of $M^{IV}TTA_4$ (M^{IV} = Zr, Hf, Ce, Th, U, Np, Pu) and $M^{III}(TTA)_4^-$ (M^{III} = Ce, Nd, Sm, Yb). *Inorg. Chem.* **2018**, *57*, 3782–3797. [CrossRef]
46. Li, X.; Hu, M.; Yin, Z.; Zhu, C.; Liu, C.-M.; Xiao, H.-P.; Feng, S. Enhanced single-ion magnetic and ferroelectric properties of mononuclear Dy(III) enantiomeric pairs through the coordination role of chiral ligands. *Chem. Commun.* **2017**, *53*, 3998–4001. [CrossRef] [PubMed]
47. Bruker APEX. *SAINT*; version 8.37A; Bruker AXS Inc.: Madison, WI, USA, 2015.
48. Sheldrick, G.M. *SADABS*, Version 2; University of Goettingen: Goettingen, Germany, 2001.
49. Sheldrick, G.M. Crystal structure refinement with SHELXL. *Acta Crystallogr. C Struct. Chem.* **2015**, *71*, 3–8. [CrossRef]
50. Macrae, C.F.; Edington, P.R.; McCabe, P.; Pidcock, E.; Shields, G.P.; Taylor, R.; Towler, T.; van de Streek, J.J. Mercury: Visualization and analysis of crystal structures. *Appl. Cryst.* **2006**, *39*, 453–457. [CrossRef]
51. Spek, A.L. *PLATON, a Multipurpose Crystallographic Tool*; Utrecht University: Utrecht, The Netherlands, 1999.
52. Jordan, R.B. Lanthanide Contraction: What is Normal? *Inorg. Chem.* **2023**, *62*, 3715–3721. [CrossRef] [PubMed]

53. Llunell, M.; Casanova, D.; Cirera, J.; Alemany, P.; Alvarez, S. *Shape Program*, Version 2; Universitat de Barcelona: Barcelona, Spain, 2010.
54. Alemany, P.; Casanova, D.; Alvarez, S.; Dryzun, C.; Avnir, D. Continuous Symmetry Measures: A New Tool in Quantum Chemistry. *Rev. Comput. Chem.* **2017**, *30*, 289–352. [CrossRef]
55. Atwood, D.A. (Ed.) *The Rare Earth Elements: Fundamentals and Applications*, 2nd ed.; John Wiley & Sons Ltd.: Singapore, Singapore, 2012.
56. Zhu, W.-H.; Xiong, X.; Gao, S.; Li, S.; Zhang, Y.; Wang, J.; Zhang, C.; Powell, A.K.; Gao, S. A family of one-dimensional lanthanide complexes bridged by two distinct carboxylate ligands with the Dy analogue displaying magnetic relaxation behavior. *Dalton Trans.* **2017**, *46*, 14114–14121. [CrossRef]
57. Aubin, S.M.J.; Sun, Z.; Pardi, L.; Krzystek, J.; Folting, K.; Brunel, L.-C.; Rheingold, A.L.; Christou, G.; Hendrickson, D.N. Reduced Anionic Mn_{12} Molecules with Half-Integer Ground States as Single-Molecule Magnets. *Inorg. Chem.* **1999**, *38*, 5329–5340. [CrossRef]
58. Guo, Y.-N.; Xu, G.-F.; Guo, Y.; Tang, J. Relaxation dynamics of dysprosium(III) single molecule magnets. *Dalton Trans.* **2011**, *40*, 9953–9963. [CrossRef]
59. Kuruvilla, E.; Joseph, J.; Ramaiah, D. Novel bifunctional acridine-acridinium conjugates: Synthesis and study of their chromophore-selective electron-transfer and DNA-binding properties. *J. Phys. Chem. B* **2005**, *109*, 21997–22002. [CrossRef] [PubMed]
60. Yang, X.-G.; Zhai, Z.-M.; Lu, X.-M.; Ma, L.-F.; Yan, D. Fast Crystallization-Deposition of Orderly Molecule Level Heterojunction Thin Films Showing Tunable Up-Conversion and Ultrahigh Photoelectric Response. *ACS Cent. Sci.* **2020**, *6*, 1169–1178. [CrossRef] [PubMed]
61. Yang, X.; Ma, L.-F.; Yan, D. Facile synthesis of 1D organic–inorganic perovskite micro-belts with high water stability for sensing and photonic applications. *Chem. Sci.* **2019**, *10*, 4567–4572. [CrossRef] [PubMed]